



# Long-term change in the source contribution to surface ozone over Japan

Tatsuya Nagashima<sup>1</sup>, Kengo Sudo<sup>2,3</sup>, Hajime Akimoto<sup>1</sup>, Junichi Kurokawa<sup>4</sup>, and Toshimasa Ohara<sup>1</sup>

<sup>1</sup>National Institute for Environmental Studies, Tsukuba, Japan

<sup>2</sup>Graduate School of Environmental Studies, Nagoya University, Nagoya, Japan

<sup>3</sup>Frontier Research Center for Global Change, Yokohama, Japan

<sup>4</sup>Asia Center for Air Pollution Research, Niigata, Japan

Correspondence to: Tatsuya Nagashima (nagashima.tatsuya@nies.go.jp)

Received: 2 December 2016 – Discussion started: 19 January 2017

Revised: 5 May 2017 – Accepted: 28 May 2017 – Published: 7 July 2017

**Abstract.** The relative contributions of various source regions to the long-term (1980–2005) increasing trend in surface ozone ( $O_3$ ) over Japan were estimated by a series of tracer-tagging simulations using a global chemical transport model. The model simulated the observed increasing trend in surface  $O_3$ , including its seasonal variation and geographical features, in Japan well and demonstrated the relative roles of different source regions in forming this trend. Most of the increasing trend in surface  $O_3$  over Japan ( $\sim 97\%$ ) that was simulated was explained as the sum of trends in contributions of different regions to photochemical  $O_3$  production. The increasing trend in  $O_3$  produced in China accounted for 36% of the total increasing trend and those in the other northeast Asian regions (the Korean Peninsula, coastal regions in East Asia, and Japan) each accounted for about 12–15%. Furthermore, the contributions of  $O_3$  created in the entire free troposphere and in western, southern, and southeastern Asian regions also increased, and their increasing trends accounted for 16 and 7% of the total trend, respectively. The impact of interannual variations in climate, in methane concentration, and in emission of  $O_3$  precursors from different source regions on the relative contributions of  $O_3$  created in each region estimated above was also investigated. The variation of climate and the increase in methane concentration together caused the increase of photochemical  $O_3$  production in several regions, and represented about 19% of the total increasing trend in surface  $O_3$  over Japan. The increase in emission of  $O_3$  precursors in China caused an increase of photochemical  $O_3$  production not only in China itself but also in the other northeast Asian regions and accounted for about 46%

of the total increase in surface  $O_3$  over Japan. Similarly, the relative impact of  $O_3$  precursor emission changes in the Korean Peninsula and Japan were estimated as about 16 and 4% of the total increasing trend, respectively. The  $O_3$  precursor emission change in regions other than northeast Asia caused increases in surface  $O_3$  over Japan mainly through increasing photochemical  $O_3$  production in western, southern, and southeast Asia and the free troposphere and accounted for about 16% of the total.

## 1 Introduction

Tropospheric ozone ( $O_3$ ) is an oxidant and photodissociates to generate the hydroxyl radical that strongly oxidizes many atmospheric compounds, including various air pollutants, and thus removes them from the atmosphere. In contrast, high levels of  $O_3$  are a major air pollutant and cause adverse effects on human health, natural vegetation, and agricultural produce (Wang and Mauzerall, 2004; Mauzerall et al., 2005; US EPA, 2006; Silva et al., 2013). Moreover, tropospheric  $O_3$  is a major greenhouse gas in the atmosphere, and reduction of its amount was recently recognized as an effective measure to mitigate near-term climate change (UNEP and WMO, 2011; Shindell et al., 2012). Therefore, the spatial and temporal variations in tropospheric  $O_3$  have always been a matter of scientific and public concern.

Japan experienced a rapid industrialization ahead of other Asian countries, and an increasing trend has been found in various observations of  $O_3$  over the past 40 years. Routine

ozonesonde measurements since 1970 at the three Japanese sites of Sapporo (43° N), Tsukuba (36° N), and Kagoshima (32° N) showed an increasing trend in O<sub>3</sub> concentration in the lowermost troposphere up to about 1990 and a relatively stable trend thereafter, with the largest increase near the ground and discernible from about 300 hPa height and below (Logan et al., 1999; Oltmans et al., 2006). With an air mass classification method based on backward air trajectories, Naja and Akimoto (2004) showed that a significant number of the air masses reaching these ozonesonde sites in Japan spend substantial time over polluted regions in East Asia. The O<sub>3</sub> levels in these regionally polluted air masses increased from the 1970s to the 1990s, mainly due to large increases in nitrogen oxide (NO<sub>x</sub> = NO + NO<sub>2</sub>) emissions over China in the 1990s. Oltmans et al. (2013) analyzed a rather short period of data (1991–2010) obtained at the Ryori (39° N) surface site in northeastern Japan and showed an increase into the mid-1990s followed by relatively little change. Other ground-based observations at a mountain site (Mt. Happo, 36° N, 1850 m a.s.l.) and three sites in the marine boundary layer along the west coast of Japan (Rishiri (45° N), Tappi (41° N), and Sado (38° N)), where few sources of pollutants exist nearby, obtained under the monitoring network of EANET (the Acid Deposition Monitoring Network in East Asia), also showed increasing trends in O<sub>3</sub> concentrations at least until the mid-2000s (Tanimoto, 2009; Tanimoto et al., 2009; Parrish et al., 2012). During the last decades, an increasing trend in tropospheric O<sub>3</sub> has also been observed at many locations in East Asia, including Taiwan (Chou et al., 2006; Chang and Lee, 2007; Li et al., 2010; Lin et al., 2010), mainland China (Lu and Wang, 2006; Ding et al., 2008; Xu et al., 2008; Wang et al., 2009; Zhang et al., 2014), and South Korea (Susaya et al., 2013; Lee et al., 2014; Seo et al., 2014). The increase rates of O<sub>3</sub> in these East Asian regions significantly vary depending on location and season in the range of about 0.3–3 ppbv yr<sup>-1</sup>; however, the increases are generally larger than the trends in tropospheric O<sub>3</sub> for other regions in the world (Cooper et al., 2014).

In Japan, analysis of long-term observations by the ambient air quality monitoring network mainly established in urban–suburban regions also showed continuous increases in surface O<sub>3</sub> from the mid-1980s until the present (Ohara and Sakata, 2003; Ohara et al., 2008; Kurokawa et al., 2009; MOE Japan, 2013; Wakamatsu et al., 2013; Akimoto et al., 2015). The consequent high violation rate of national ambient air quality standard (AAQS) for surface O<sub>3</sub> (hourly mean concentration of 60 ppbv) has also been a persistent issue in environmental administration for a long time. Therefore, there is an urgent need to study the reason for the increasing trend and examine the countermeasures. One clue is that the simultaneous observations of O<sub>3</sub> precursors such as NO<sub>x</sub> and non-methane hydrocarbons (NMHCs) by this monitoring network revealed their decreasing trends in the same period (MOE Japan, 2013), which seemed inconsistent with the increasing trend in O<sub>3</sub> over Japan. These observed features

of O<sub>3</sub>-related atmospheric species in Japan suggest that there should be an influence of transboundary transport from outside of Japan on the recent increasing trend in O<sub>3</sub>. The influence of transboundary transport on surface O<sub>3</sub> in East Asia was examined in several studies (Sudo and Akimoto, 2007; Li et al., 2008; Nagashima et al., 2010; Wang et al., 2011). Nagashima et al. (2010) demonstrated that the O<sub>3</sub> transported from outside of Japan accounted for more than 70 % of surface O<sub>3</sub> over Japan in the cold season (October–March) during 2000–2005, and most was attributable to O<sub>3</sub> from distant sources outside East Asia and from the stratosphere. In the warm season (April–September), the contribution of domestically created O<sub>3</sub> in Japan to surface O<sub>3</sub> over Japan increased significantly (about 20–40 %). The short-range intra-regional transport of O<sub>3</sub> from other parts of East Asia still contributed about 25 %, and long range inter-regional transport of O<sub>3</sub> from outside East Asia and the stratosphere, particularly in spring, could account for about half of surface O<sub>3</sub> over Japan.

Therefore, the influence of O<sub>3</sub> from source regions outside and inside East Asia and the stratosphere should be considered to explain the cause of the increasing trend in surface O<sub>3</sub> over Japan. The rapid increase in O<sub>3</sub> precursor emissions in East Asia in recent decades (Ohara et al., 2007; Kurokawa et al., 2013) was demonstrated as a major cause of the increasing trend in springtime O<sub>3</sub> over Japan by comparing regional chemical transport model (CTM) simulations of recent decades with and without the East Asian O<sub>3</sub> precursor emission increases during the period (Kurokawa et al., 2009; Tanimoto et al., 2009). However, they only showed the springtime O<sub>3</sub> case and it was unclear whether the relationship held in other seasons. Moreover, the relative contributions of individual countries or regions in East Asia have not been well examined, particularly concerning increased surface O<sub>3</sub> over Japan.

Here, we investigated the cause of the continuous increase in surface O<sub>3</sub> over Japan reported in the literature above, focusing on the relative contributions of various source regions over the globe, particularly the contributions of individual regions in East Asia, with a long-term simulation of a global CTM using the tagged tracer method. Using the same model and method, Nagashima et al. (2010) showed such relative contributions of regions inside and outside East Asia to surface O<sub>3</sub> over Japan as average values for the early 2000s. The current study investigated the temporal evolution of the relative contributions of each region for the 26 years from 1980 to 2005.

## 2 Methods

### 2.1 Model description

In this study, we employed a chemistry climate model (CCM), CHASER (Sudo et al., 2002), developed for atmospheric chemistry research in the troposphere. The basic set-

ting of the model was almost identical to that used by Nagashima et al. (2010). However, the horizontal resolution was modified from T63 (about 1.9° by 1.9° grid spacing in longitude and latitude) to T42 (about 2.8° by 2.8°) because a longer simulation period was necessary than in the previous study, and so the cost of computation was reduced in the present study by selecting lower horizontal resolution. There were 32 vertical layers with the top layer set at approximately 40 km altitude. A detailed tropospheric photochemistry consisted of 113 chemical reactions and 27 photodissociations involving O<sub>3</sub>, HO<sub>x</sub>, NO<sub>x</sub>, methane (CH<sub>4</sub>), CO, and NMHCs calculated the temporal evolution in the concentrations of 53 chemical species. The concentrations of O<sub>3</sub> and some nitrogen compounds (NO<sub>x</sub>, HNO<sub>3</sub>, and N<sub>2</sub>O<sub>5</sub>) above the tropopause that should affect tropospheric chemistry were assimilated into the monthly mean output data of stratospheric CCM because the version of CHASER used was unable to calculate several chemical processes, such as halogen-related chemical reactions, which are indispensable for realistic representation of such chemical compounds in the stratosphere. The model also included dry and wet deposition of chemical species.

In this study, we conducted tracer-tagging simulation by using two different setups (full chemistry and tracer transport) of CHASER. The full-chemistry setup calculated the actual temporal change in the concentration of chemical species through the abovementioned chemical and physical processes and outputted the chemical production and loss tendencies of O<sub>3</sub> and related species. Then, the tracer-transport setup used the outputted chemical tendencies to calculate the temporal change in the concentration of hypothetical O<sub>3</sub> tracers. In the following subsection, the calculation procedure is briefly described.

## 2.2 Outline of the numerical simulations

### 2.2.1 Forcings for long-term simulation

Long-term simulation was performed for the period 1980–2005. The end of the simulation period (2005) was determined mainly due to the temporal coverage of the Asian emission data described below; however, this period sufficiently covered the years reported to have an increasing trend in surface O<sub>3</sub> over Japan in previous literature. To drive the physical properties of the model for this 26-year period, the temperature and horizontal wind velocities in the model were assimilated into the National Center for Environmental Prediction/National Center of Atmospheric Research (NCEP/NCAR) 6 h reanalysis data (Kalnay et al., 1996) of the corresponding year, and sea surface temperature and sea ice data of the Hadley Centre's Sea Ice and Sea Surface Temperature (HadISST) data set (Rayner et al., 2003) were used in the model.

The monthly mean stratospheric O<sub>3</sub> data of Akiyoshi et al. (2009) were used for the assimilation above the

tropopause for this period. These data were the output of a stratospheric CCM simulation according to the hindcasting scenario for 1980–2004 (REF1 scenario) of the CCM validation activity (CCMVal) (Eyring et al., 2005) and included an interannual variation (IAV) associated with the 11-year solar cycle and large declines after 1982 and 1991 due to the El Chichón and Pinatubo eruptions, respectively, in addition to a continuous decreasing trend during the whole period. Although the simulated declines in stratospheric O<sub>3</sub> due to the two large volcanic eruptions were somewhat overestimated, the simulated IAVs in stratospheric O<sub>3</sub> represented those observed with a total ozone mapping spectrometer (TOMS) from satellites reasonably well (Akiyoshi et al., 2009). Incidentally, the stratospheric O<sub>3</sub> data of 2004 were used for 2005.

The long-term variation in the emissions of O<sub>3</sub> precursors (NO<sub>x</sub>, CO, and NMHCs) were taken from multiple emission inventories. For anthropogenic emissions in Asia, the Regional Emission inventory in ASia (REAS ver.1.2) (Ohara et al., 2007) was used for each year over the whole simulation period (1980–2005). Kurokawa et al. (2009) used these emission data with a regional air quality model that represented the interannual variability in surface O<sub>3</sub> over Japan for a similar period (1981–2005) to the present study well. For anthropogenic emissions outside Asia, a combination of three versions of EDGAR (Emission Database for Global Atmospheric Research) emission data was used: EDGAR-HYDE (Van Aardenne et al., 2001) for 1980 and 1990, EDGAR v3.2 (Olivier and Berdowski, 2001) for 1990 and 1995, and EDGAR v3.2 Fast Track 2000 (FT2000) (Olivier and Berdowski, 2001) for 2000. Because several emission sectors considered in EDGAR v3.2 were not considered in EDGAR-HYDE, the emissions for 1990 in EDGAR-HYDE were generally smaller than in EDGAR v3.2. Therefore, we used EDGAR v3.2 data for 1990, and also scaled them to estimate emission data for 1980 rather than simply using EDGAR-HYDE data for 1980. For this purpose, we scaled EDGAR v3.2 data for 1990 so that the ratio ( $r$ ) of the difference between 1980 ( $f_1$ ) and 1990 data ( $f_2$ ) and their average in EDGAR-HYDE (i.e.,  $r = (f_2 - f_1)/(f_1 + f_2)/2$ ) equaled the corresponding ratio ( $R$ ) calculated from 1990 data in EDGAR v3.2 ( $F_2$ ) and 1980 data scaled from it ( $F_1$ ) (i.e.,  $R = (F_2 - F_1)/(F_1 + F_2)/2$ ). We calculated  $F_1$  from the known values of  $f_1$ ,  $f_2$ , and  $F_2$  using the equation  $r = R$ . Since EDGAR emission data were not available for each year but for every 10 or 5 years in the simulation period, the emissions for intermediate years were interpolated, and FT2000 data were used for years after 2000. The vegetation fire emission data developed in the RETRO (REanalysis of the TROpospheric chemical composition over the past 40 years) project (Schultz et al., 2008) were used for O<sub>3</sub> precursor emissions from biomass burning for each year until 2000 in the simulation period, and data for 2000 were used for years after 2000. Historical transition of the atmospheric concentrations of carbon dioxide, nitrous oxide, and CH<sub>4</sub>

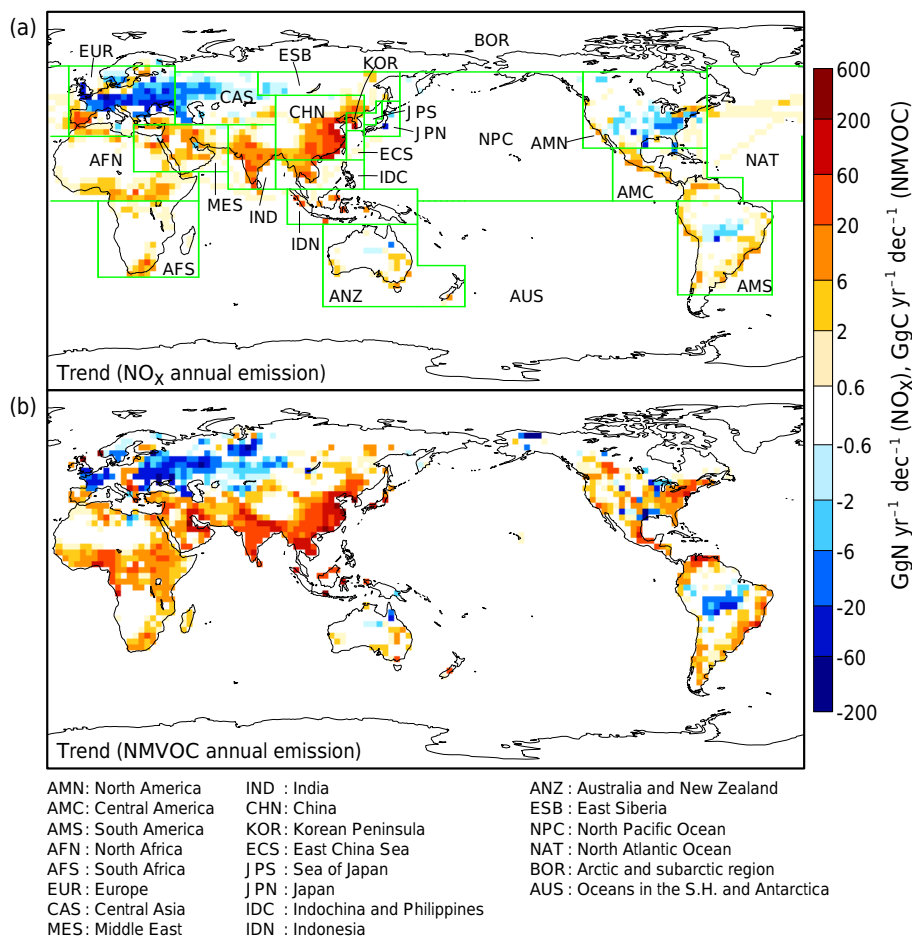


**Figure 1.** Linear trends in (a)  $\text{NO}_x$  and (b) NMVOC emissions during the simulation period (1980–2005) used in the study. Significant trends at 5 % risk level are colored. Source regions for tracer tagging are also displayed in the top figure.

were prescribed with those used in Nozawa et al. (2005), which were somewhat old estimations of the historical evolution in greenhouse gas concentrations, but not much different from recent estimations such as for the Representative Concentration Pathways (RCPs) (Meinshausen et al., 2011). The difference in the concentrations between both estimations were generally within a couple of percentages in the simulation period.

The linear trends in  $\text{NO}_x$  and non-methane volatile organic compound (NMVOC) annual emissions used in this study in the simulation period of 1980–2005 are shown in Fig. 1. The long-term trends in emissions of both species showed generally similar geographical features to each other: large decrease trends in central Europe, Scandinavia, western Russia, and Kazakhstan, whereas there were widely spread increasing emissions in western, southern, southeastern, and East Asia, almost all of Africa and Central and South America except for inland Brazil. In North America,  $\text{NO}_x$  emission generally decreased in the simulation period except for the west coast and New England in the USA, but that of

NMVOC mostly increased with a few patchy exceptions. The trends in  $\text{NO}_x$  and NMVOC emissions mentioned above were mainly due to the change in anthropogenic emissions, while the change in biomass burning emissions led to a discernible trend in several regions such as inland Brazil and the south of Sahel.

The long-term evolution of annual emissions of  $\text{NO}_x$  and NMVOC over several source areas in the Northern Hemisphere is shown in Fig. 2. Because the emission data were the combination of three different datasets outside Asia, there were somewhat discontinuous changes at the joint years (1990 and 1995) in European and North American emissions. The emissions of  $\text{NO}_x$  and NMVOC over Europe had peaks around 1990 and generally decreased afterward. Over North America, both species showed small long-term trends: slight decreases in  $\text{NO}_x$  and slight increases in NMVOC emissions. The emissions of both species over China greatly increased during the whole period. The  $\text{NO}_x$  emissions were about 4.0 times larger in 2005 than 1980 and correspondingly NMVOC was 2.5 times larger, which made emissions

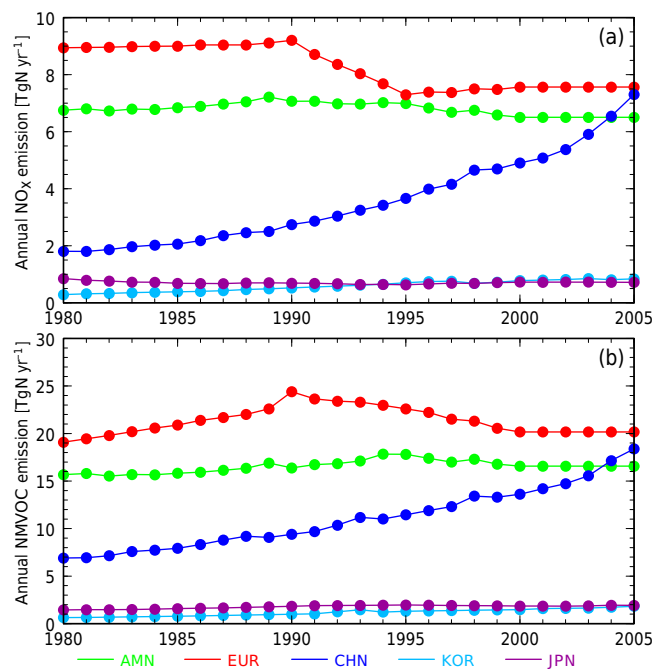


**Figure 2.** Temporal evolution of emissions of (a) NO<sub>x</sub> and (b) NMVOC averaged over several source areas in the Northern Hemisphere depicted in Fig. 1.

of both species for China equal to or even surpassing those for Europe or North America in 2005. The emissions of both species over the Korean Peninsula (KOR) were approximately 2.8 times larger in 2005 than in 1980. However, those over Japan showed no such increase: NO<sub>x</sub> emission decreased until 1995 and thereafter remained stable, whereas NMVOC emissions went up until 1995 and then slightly decreased.

### 2.2.2 Tracer tagging

We conducted a 26-year simulation using the full-chemistry setup of CHASER with all the forcings mentioned above, followed by another 26-year simulation with the tracer-transport setup of CHASER, which calculated the concentration of hypothetical O<sub>3</sub> tracers, each tagged with a particular region in the model domain. The procedure to tag a tracer with each region in the second simulation was the same as that used by Nagashima et al. (2010) and a brief description follows. In the second simulation, the transport and dry deposition of each O<sub>3</sub> tracer were calculated the same as in the first simulation; however, the chemical development of tracers was calculated using the chemical production ( $P$ ) and loss frequencies ( $L$ ) of the extended odd oxygen family ( $O_x = O_3 + O + O(^1D) + NO_2 + 2NO_3 + 3N_2O_5 + PANs + HNO_3 + \text{other nitrates}$ ) calculated and archived in the first simulation. In the first simulation, 3-D fields of  $P$  and  $L$  were outputted every 6 h. Each O<sub>3</sub> tracer could be lost

chemically everywhere in the model domain at the frequency of  $L$ , but could be chemically produced only inside its tagged region. In the stratosphere, the concentration of O<sub>3</sub> tracer tagged with the stratosphere was assimilated into the same stratospheric O<sub>3</sub> data as used in the first simulation, but the concentration of the tracers tagged with the region in the troposphere were all set to zero. The calculated concentration of each tagged O<sub>3</sub> tracer at a given location represents the contribution of O<sub>3</sub> produced in each source region and transported to that location.

The troposphere in the model domain was horizontally separated into 22 regions and each horizontal region was further separated vertically between the free troposphere (FT) and the planetary boundary layer (PBL). The stratosphere was considered one separate source region, that is, the model domain was separated into 45 source regions. The 22 regions for horizontal separation are shown in Fig. 1 and each region was assigned a three-letter code (e.g., AMN for North America), which is used in the following sections. For the vertical separation of the source regions in the troposphere, the PBL was defined as the lowest six layers in the model (surface to about 750 hPa), based on the observed and modeled vertical profiles of O<sub>3</sub> production.

The long-term tracer-tagging simulation allowed estimation of the long-term variations in contributions of each source region to the O<sub>3</sub> concentration at given receptor locations. This is important information to explain the cause of the reported increasing trend in surface O<sub>3</sub> over East Asia. However, it should be noted that the tracer-tagging simulation calculates the amount of O<sub>3</sub> in a receptor location that was produced chemically in each source region from O<sub>3</sub> precursors emitted from both the source region and adjacent source regions. Thus, the contribution of a source region estimated in the tracer-tagging simulation should not be fully attributed to emissions of O<sub>3</sub> precursors in that source region. Emission sensitivity simulation is another method of estimating the portion of O<sub>3</sub> fully attributable to a change in O<sub>3</sub> precursor emissions in a source region and takes the difference of simulated O<sub>3</sub> between two model runs with and without perturbed O<sub>3</sub> precursor emissions in that source region. The resulting estimations of source contributions by the two methods can differ; however, the differences have not yet been well quantified. Li et al. (2008) reported that the difference between the two methods could be as much as 30 % in source apportionment estimation for one location and time (i.e., Mt. Tai in central eastern China in June 2006). Wang et al. (2011) found somewhat larger differences in the contributions of China to domestic O<sub>3</sub> concentration between the two methods for each month of the year, but no discussions were made for O<sub>3</sub> over Japan.

Nevertheless, we employed the tracer-tagging simulation to study the cause of reported long-term change in surface O<sub>3</sub> over Japan mainly due to its computational efficiency. Thus, the results should be carefully interpreted in terms of the difference between the source regions of chemical O<sub>3</sub> produc-

tion and those of  $O_3$  precursor emissions. The computational efficiency resulting from the tracer-tagging approach and relatively coarse horizontal resolution enabled us to make several sensitivity simulations with the different combination of forcings for long-term simulation. In the following sections, the simulation with the full set of long-term forcings described above, hereinafter referred to as the “standard” simulation, is initially analyzed. This is then further interpreted using the results of sensitivity simulations; the specific settings of sensitivity simulations are also described.

### 3 Results and discussion

#### 3.1 Long-term evolution of surface $O_3$ over Japan

Nagashima et al. (2010) validated how well CHASER can reproduce the observed features of surface  $O_3$  concentrations by comparing the simulated surface  $O_3$  concentrations with observations taken during 2000–2005 at several sites mainly in rural areas in the Northern Hemisphere, and CHASER successfully simulated the annual variation in surface  $O_3$  in a variety of regions. In this study, the horizontal resolution of the model differed from that used in Nagashima et al. (2010); however, the model represented the observed concentrations and seasonal evolutions of surface  $O_3$  well (Fig. S1 and Table S1 in the Supplement). Surface  $O_3$  over Japan has been observed at ambient air quality monitoring stations since the early 1970s. The monitoring data were compiled by the Atmospheric Environmental Regional Observation System (AEROS). About 1000 monitoring stations widely distributed throughout Japan, except on the southern islands, could be used for validation of the model results. The monitoring data of AEROS have been used to examine the long-term variation in surface  $O_3$  over Japan in several studies and showed significant increasing trends (Ohara and Sakata, 2003; Ohara et al., 2008; Kurokawa et al., 2009; Akimoto et al., 2015). We validated the simulated surface  $O_3$  over Japan with the AEROS data in terms of the long-term variation in the following.

For the validation, the monitoring sites selected had continuously observed the surface  $O_3$  during the simulation period (1980–2005). To ensure continuity of sites, we selected monitoring sites with annual mean surface  $O_3$  available for every year in the simulation period. The annual mean data at a monitoring site were calculated as the average of monthly means when available for more than 9 months, the monthly mean was calculated from daily means when available for over 19 day month<sup>-1</sup>, and the daily mean was calculated from hourly means when available for more than 19 h day<sup>-1</sup>. There were 339 sites, located mainly in populated areas of Japan, except on the northernmost island (Hokkaido) and southern islands (Ryukyu Islands). We first calculated the annual mean surface  $O_3$ , and then the annual means of all sites were averaged to calculate the observed annual mean sur-

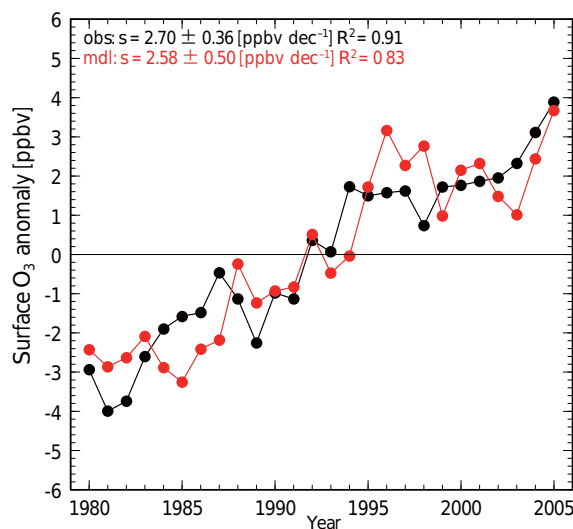


**Figure 3.** The temporal changes in annual mean surface  $O_3$  anomaly averaged over Japan from observation (AEROS: black) and model calculations (red). Anomalies are defined as deviations from the values averaged over 1980–2005. The slope of a regression ( $s$ ) for 1980–2005 with its 95 % confidence interval and  $R^2$  are also shown.

face  $O_3$  over Japan. The simulated annual mean surface  $O_3$  over Japan was calculated as the average of annual means of the model grids, which included the locations of monitoring sites selected for the validation. The temporal variations in observed and simulated annual mean surface  $O_3$  anomalies during 1980–2005 averaged over Japan are shown in Fig. 3. During the period, the observed annual mean surface  $O_3$  over Japan showed a clear increasing trend with a linear increase of about 2.70 ppbv decade<sup>-1</sup>, which was significant at the 5 % risk level. The simulated annual mean surface  $O_3$  over Japan also showed a significant increasing trend with a rate of about 2.58 ppbv decade<sup>-1</sup>, which corresponded well to the observed increase in surface  $O_3$  over Japan. The value of the linear increasing trend and the observed features of long-term variation in surface  $O_3$  over Japan – such as a rapid increase from the mid-1980s to the mid-1990s followed by a stagnation of increase for about 7–8 years and a further increase in the past several years – were reasonably well captured by the model.

The model also represented the longitudinal differences in the long-term trend in surface  $O_3$  in Japan well. Figure 4 shows the maps of linear trends in annual mean surface  $O_3$  during 1980–2005 calculated from the model simulations and observations at AEROS monitoring sites as selected for Fig. 3. The simulated annual mean surface  $O_3$  showed an increasing trend in the whole area, including all of Japan and the Korean Peninsula (Fig. 4a). The simulated increasing trend in annual mean surface  $O_3$  well exceeded 2.0 ppbv decade<sup>-1</sup> in wide areas of Japan except for Hokkaido and tended to be greater toward western Japan,

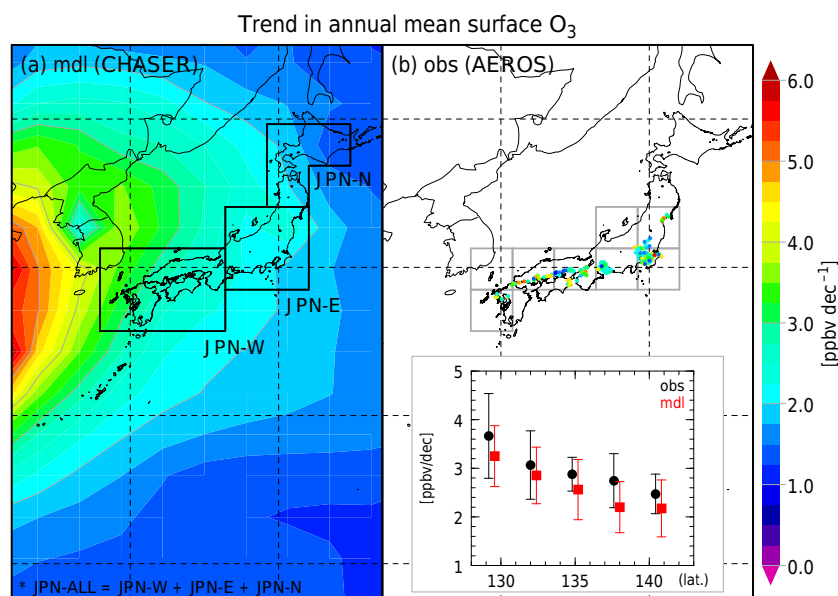


**Figure 4.** The linear trend in annual mean surface  $O_3$  in 1980–2005 calculated from (a) model simulations and (b) observations at AEROS monitoring sites. The inset in (b) shows the longitudinal change in linear trends (black: AEROS observation; red: model) averaged within the model grids shown by gray rectangles. The error bars denote their 95 % confidence intervals. The black-rimmed areas in (a) are the areas for averaging used in the figures from Fig. 6. Note that JPN-ALL is the sum of the JPN-W, JPN-E, and JPN-N areas and was used for the averaging in those figures.

which is nearer to the Asian continent. However, the increasing trends in observed annual mean surface  $O_3$  at each monitoring site (Fig. 4b) differed greatly from each other even at nearby sites, and there was no apparent longitudinal tendency in trends at individual monitoring sites. However, we averaged the observed annual mean surface  $O_3$  at individual monitoring sites at longitudinal intervals (approximately  $2.8^\circ$ ) of the model grids as shown by gray rectangles (Fig. 4b) and calculated the long-term trend in averaged monitoring data at each longitudinal band. The calculated increasing trends were clearly larger toward the west, which was consistent with the westward rise of the increasing trends in simulated data.

There were seasonal differences in the long-term increasing trend in surface  $O_3$  over Japan. The temporal variations in observed and simulated seasonal mean surface  $O_3$  anomalies during 1980–2005 averaged over Japan are shown in Fig. 5. The increasing trend in surface  $O_3$  over Japan in the monitoring data was greatest in spring (March–May:  $4.04 \text{ ppbv yr}^{-1}$ ) and was also large in summer (June–August:  $3.07 \text{ ppbv yr}^{-1}$ ); in contrast, increasing trends were relatively small in fall (September–November:  $2.29 \text{ ppbv yr}^{-1}$ ) and winter (December–February:  $1.28 \text{ ppbv yr}^{-1}$ ). Seasonal dependency in the increasing trends in observed surface  $O_3$  over Japan has been previously reported (Ohara and Sakata, 2003; Parrish et al., 2012). Ohara and Sakata (2003) examined almost the same  $O_3$  monitoring data in Japan as used in the present study for the period 1985–1999 and showed a

year-round increase in surface  $O_3$  from 1985–1987 to 1997–1999, with a greater increase in the warm season (March–August) than in the rest of the year. Parrish et al. (2012) summarized long-term changes in lower tropospheric baseline  $O_3$  over the world, including two regions in Japan (Mt. Happon and several sites in the marine boundary layer grouped as one region), and showed that the increasing trend in surface  $O_3$  was greatest in spring and least in fall in these two regions. In the present study, the simulated increasing trend in seasonal mean surface  $O_3$  was also larger in the warm (spring–summer) than in the cold season (fall–winter), consistent with the observed increasing trends.

As described above, our model captured the basic features of long-term trends in observed surface  $O_3$  over Japan well, which allowed us to use the simulated data for further analysis on the source of the long-term trend in the next section.

### 3.2 Contributions of $O_3$ production regions

The tracer-tagging simulation for 1980–2005 was conducted, and the IAVs in the annual mean concentrations of each tagged  $O_3$  tracer averaged over Japan are shown in Fig. 6. The tagged tracers other than the FT and stratosphere in Fig. 6 and the following figures represent the contribution of  $O_3$  produced in the PBL of different source regions shown in Fig. 1, where contributions of several source regions were grouped into some combined source regions. It should be noted that the model grids used for averaging in these figures differed from those in Figs. 3–5. They encompassed almost

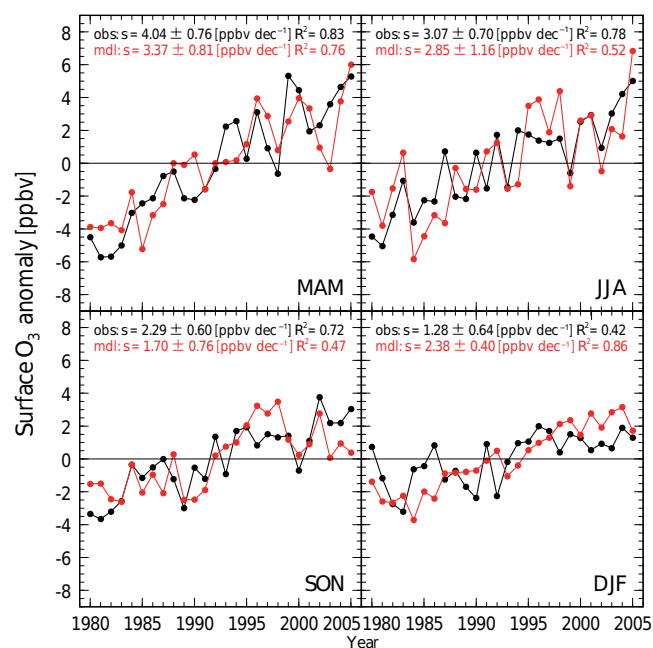


**Figure 5.** Same as Fig. 3 but showing the temporal changes in seasonal mean surface O<sub>3</sub> anomaly averaged over Japan from observations (AEROS: black) and model calculations (red).

all of Japan, excluding the Ryukyu Islands in order to examine temporal behavior of tagged O<sub>3</sub> tracers in all of Japan (see Fig. 4 for actual areas for averaging).

Domestically created O<sub>3</sub> was the largest contribution to surface O<sub>3</sub> concentration averaged over Japan during the whole simulation period. The contribution of domestic production had a large IAV and was larger in the last decade (1996–2005) than previously.

The second largest contribution was the O<sub>3</sub> created in the FT as a whole during almost the entire period. For the FT, the northern midlatitude regions such as the North Pacific (NPC), Europe (EUR), North Atlantic (NAT), North America (AMN), and China (CHN) made leading contributions during the period; however, the increasing trend in these contributions was considerable, particularly for CHN and NPC (Fig. S2). Despite such differences among the regional contributions in the FT, we hereafter only considered the total of each regional contribution in the FT since it was difficult to associate a regional contribution with a particular source region of O<sub>3</sub> precursor emissions. The precursors eventually resulted in O<sub>3</sub> production in a region in the FT being transported a longer distance due to faster wind speed in the FT and would therefore be influenced by emissions from a wider range of source regions than in the PBL. The total FT contribution showed an increasing trend during the period.

The NO<sub>x</sub> emission from lightning was an indispensable source of NO<sub>x</sub> in the FT. The global annual lightning-NO<sub>x</sub> emission in the current simulation was about 3.1 TgN yr<sup>-1</sup> averaged over the entire period and showed a small but sig-

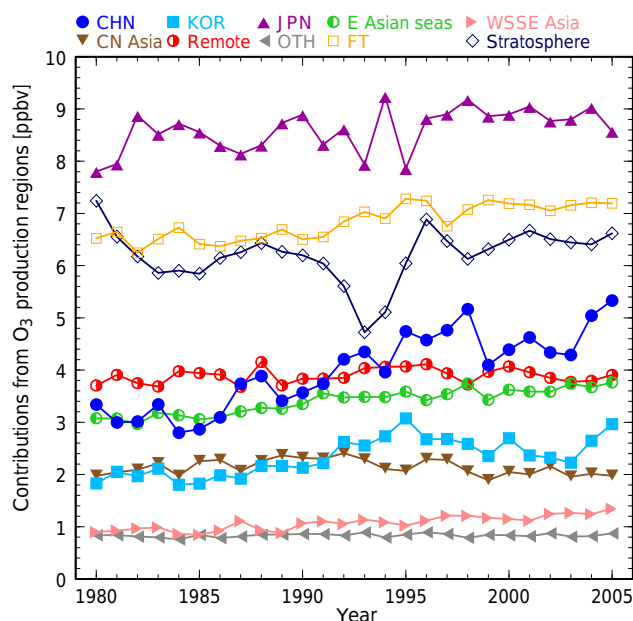


**Figure 6.** Long-term changes in annual mean contributions from source regions to surface O<sub>3</sub> over Japan. Some source regions are grouped: E Asian seas is the sum of NPC, JPS, and ECS; WSSE Asia is the sum of MES, IND, IDN, and IDC; CN Asia is the sum of CAS and ESB; Remote is the sum of AMN, NAT, and EUR; and OTH is the other regions in the planetary boundary layer.

nificant increase of about 0.012 TgN yr<sup>-1</sup> (0.39 % yr<sup>-1</sup>). The increase in lightning-NO<sub>x</sub> emission was a consequence of changes in convection activities due to the change in climate forced into the model during the period. However, this increase in lightning-NO<sub>x</sub> emission was not the main cause of the increase in the contribution of the total FT because a sensitivity simulation with all emissions, CH<sub>4</sub> concentration, and stratospheric O<sub>3</sub> fixed at the year 1980 level but with the same temporal evolution in climate showed a quite similar increase in lightning-NO<sub>x</sub> emission but no significant increasing trend in the total FT contribution. Therefore, the main cause of the increasing trend in the total FT contribution was likely to be factors other than the increase in lightning-NO<sub>x</sub> emission.

The contribution of stratospheric O<sub>3</sub> was also large during the entire period, with considerable temporal fluctuations. The large decreases in stratospheric contribution in the early 1980s and 1990s stemmed from the decline of stratospheric O<sub>3</sub> concentration due to the impact of large volcanic eruptions of El Chichón in 1982 and Mt. Pinatubo in 1991 (Akiyoshi et al., 2009).

In the early 1980s, the combined contributions of remote regions far from Japan in the northern midlatitude (Remote: EUR, NAT, and AMN) made a significant contribution, the fourth largest, to the surface O<sub>3</sub> over Japan and remained at a steady level of contribution during the study period. At the same time, the contribution of CHN significantly increased

from the mid-1980s, overtook the contribution of Remote in the early 1990s, and became the largest single regional contribution – excluding the domestic one (i.e., JPN). Moreover, the contributions of O<sub>3</sub> produced in KOR; the coastal regions in East Asia (E Asian seas: NPC, East China Sea (ECS), and Japan Sea (JPS)); and the western, southern, and southeastern (WSSE) Asian regions (including the Middle East (MES), India (IND), Indochina and the Philippines (IDC), and Indonesia (IDN)) also showed obvious increasing trends.

The linear trend (ppbv decade<sup>-1</sup>) of annual mean tagged O<sub>3</sub> tracers during the simulation period as well as that of the total O<sub>3</sub>, which is the sum of all tagged O<sub>3</sub> tracers averaged over whole Japan (JPN-ALL) and those averaged over three subregions in Japan: western (JPN-W), eastern (JPN-E), and northern (JPN-N) Japan is shown in Fig. 7 (see Fig. 4 for the definition of subregions). The trend was calculated from the annual mean concentrations. The increasing trend in total O<sub>3</sub> averaged over JPN-ALL was 2.37 ppbv decade<sup>-1</sup>, which was somewhat smaller than estimated in Fig. 3 (2.58 ppbv decade<sup>-1</sup>) due to inclusion of model grids in JPN-N for averaging where the simulated increasing trend in O<sub>3</sub> was relatively small. The increasing trend in total O<sub>3</sub> tended to be greater westward. The absolute contribution of domestically produced O<sub>3</sub> in Japan differed among the regions – it tended to be larger in JPN-E than other parts of Japan (Nagashima et al., 2010); however, there were no such regional differences in long-term trends. The westward tendency of larger increasing trends in total O<sub>3</sub> over Japan was mainly due to the similar tendency in the trends in the contribution of CHN, KOR, and E Asian seas, which strongly suggested a large impact of intra-regional transboundary air pollution in East Asia. In particular, the increasing trend in the CHN contribution was the largest for all subregions in Japan. The increasing trend in the contributions of total FT and WSSE Asia was slightly smaller for JPN-N than for other parts of Japan, which also contributed to the regional differences in the trend in total O<sub>3</sub> over Japan. Due to the large interannual fluctuation, the linear long-term trend in the stratospheric contribution was non-significant for all regions in Japan.

The linear trend in tagged O<sub>3</sub> tracers and total O<sub>3</sub> averaged over all of Japan in spring, summer, fall, and winter is shown in Fig. 8. The increasing trends in total O<sub>3</sub> in decreasing order were spring, summer, winter, and fall. This is quite consistent with the seasonal differences in the increasing trend in O<sub>3</sub> observed at several Japanese sites from the 1990s to 2011 (Parrish et al., 2012). The increasing trend in the CHN contribution was the largest of all contributions in all four seasons and the trend was particularly large in spring. The KOR contribution was also larger in spring than in other seasons. The contribution of the E Asian seas increased significantly in all seasons. Seasonal differences in the increasing trend in the E Asian seas contribution were small, but were slightly larger in the warm (spring–summer) than the cold season (fall–winter). The increasing trend in domestic

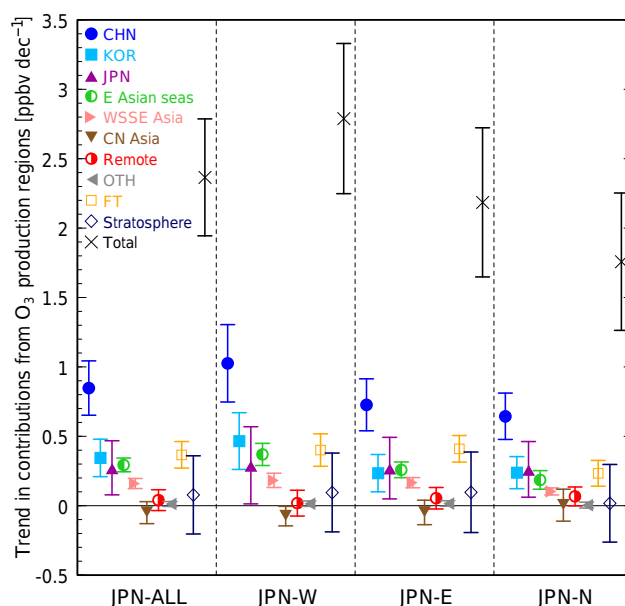


**Figure 7.** Linear trends in annual mean contributions in 1980–2005 from source regions to surface O<sub>3</sub> over Japan shown in Fig. 6 (JPN-ALL) and those averaged in three subregions in Japan (JPN-W, JPN-E, and JPN-N). Error bars are 95 % confidence intervals.

(JPN) contribution was larger in spring than in summer, similar to the cases of the CHN and KOR contributions, but trends in both seasons were non-significant, whereas those in the cold season were significantly larger than in the warm season. The FT and WSSE Asian contributions showed semi-annual change in their increasing trends: larger in summer and winter than in spring and fall. The contribution of Remote showed a significant increasing trend only in winter. The seasonal features in each regional contribution described above enabled the explanation of the cause of the seasonality of the increasing trend in total O<sub>3</sub> over Japan as follows. The largest increasing trend in total O<sub>3</sub> in spring was predominantly attributed to the large increasing trend in contributions of source regions in northeast Asia (CHN, KOR, E Asian seas, and JPN). The increasing trends in the contributions of CHN, KOR, and JPN were smaller in summer. However, they were partly compensated for by the growth of increasing trends in the FT and WSSE Asian contributions from spring to summer. In the cold season, trends for most regions were smaller than in the warm season, except for JPN. The increasing trend in contributions of northeast Asian regions differed little between fall and winter; however, those of FT, WSSE Asia, and Remote had larger increasing trends in winter than in fall, which made the increasing trend in total O<sub>3</sub> in winter larger than in fall.

Table 1 summarizes the linear trends in annual mean tagged O<sub>3</sub> tracers and the total O<sub>3</sub> averaged over JPN-ALL. The vast majority (about 97 %) of the trend in total O<sub>3</sub> was balanced with the sum of those trends in re-

**Table 1.** Summary of the linear trends in annual mean tagged O<sub>3</sub> tracers as well as the total O<sub>3</sub> averaged over Japan (JPN-ALL) for 1980–2005. Bold figures denote that trends are significant at 5% risk level.

Source region	Trend [ppbv decade <sup>-1</sup> ]	Percent
CHN	<b>0.85 ± 0.2</b>	35.8
KOR	<b>0.34 ± 0.14</b>	14.6
JPN	<b>0.27 ± 0.19</b>	11.5
E Asian seas	<b>0.29 ± 0.05</b>	12.4
WSSE Asia	<b>0.16 ± 0.04</b>	6.8
CN Asia	−0.05 ± 0.08	−2.1
Remote	0.04 ± 0.08	1.7
OTH	0.01 ± 0.02	0.5
FT	<b>0.37 ± 0.1</b>	15.5
Strat.	0.08 ± 0.28	3.3
Total	<b>2.37 ± 0.42</b>	100.0

gional contributions with statistical significance. The largest contribution was from the increase in O<sub>3</sub> produced in CHN (0.85 ppbv decade<sup>-1</sup>), which corresponded to about 36% of the increasing trend in total O<sub>3</sub>. The increasing trend in the contribution of the total FT was also large (0.37 ppbv decade<sup>-1</sup>), representing about 16% of the total O<sub>3</sub> trend. The contributions of northeast Asian regions other than CHN also increased significantly (0.34, 0.29, and 0.27 ppbv decade<sup>-1</sup> for KOR, the E Asian seas, and JPN, respectively) and each accounted for about 12–15% of the total O<sub>3</sub> trend. About 7% of the total O<sub>3</sub> trend was attributable to the increasing trend in WSSE Asian contributions (0.16 ppbv decade<sup>-1</sup>). The linear trends in the contributions of remaining regions were small and non-significant, and thus were not important concerning the cause of reported surface O<sub>3</sub> increase over Japan.

### 3.3 Impact of temporal variations in O<sub>3</sub> precursor emissions in different source regions on regional O<sub>3</sub> production

The results in the preceding section revealed the relative importance of O<sub>3</sub> produced in different regions to the recent increasing trend in surface O<sub>3</sub> over Japan. It is noteworthy that this does not indicate the relative importance of the different regions of O<sub>3</sub> precursor emissions. For example, there were significant contributions of the E Asian seas to the increasing trend in surface O<sub>3</sub> over Japan, but there were clearly no large emission sources of precursors in these maritime regions other than navigation. The increasing trend in the contribution of the E Asian seas was likely a consequence of increased transport of O<sub>3</sub> precursors to this region, which had been emitted in adjacent land areas. However, the tracer-tagging approach cannot distinguish the differences in origins of emissions of precursors that resulted in O<sub>3</sub> production in the E Asian seas. To further investigate the roles of differ-

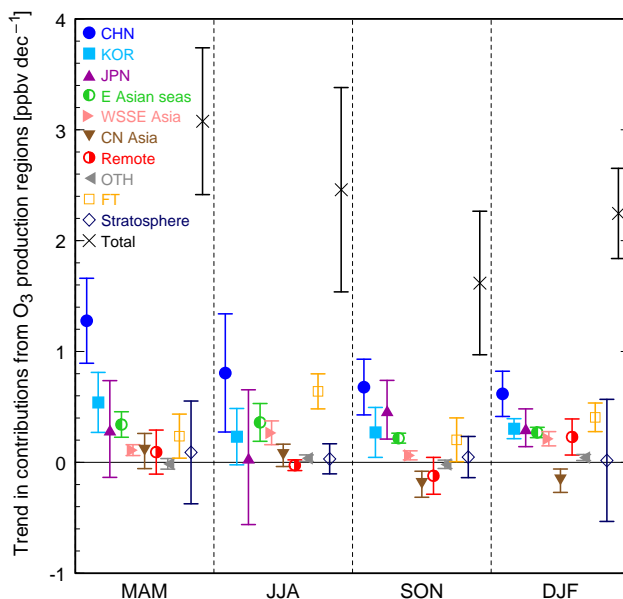


**Figure 8.** Linear trends in the contributions in 1980–2005 from source regions to surface O<sub>3</sub> over Japan in different seasons: spring (MAM), summer (JJA), fall (SON), and winter (DJF). Error bars are 95% confidence intervals.

ent regions in the recent increasing trend in surface O<sub>3</sub> over Japan, we performed a series of sensitivity simulations with different assumptions for the temporal variation in factors, which would affect the surface O<sub>3</sub> over Japan. Each sensitivity simulation consisted of a 26-year simulation with the full-chemistry setup of CHASER followed by another 26-year simulation with the tracer-tagging setup of CHASER. Initially, a sensitivity simulation was performed that was only forced by the IAVs in the climate but with all emissions of O<sub>3</sub> precursors, CH<sub>4</sub> concentration, and stratospheric O<sub>3</sub> fixed at the year 1980 level; then we gradually added the temporal variation in chemical factors as summarized in Table 2. The simulation F, driven by the temporal variation in all forcings, was identical to the standard simulation, and simulation A was mentioned concerning lightning-NO<sub>x</sub> emission in the preceding section (Sect. 3.2).

The linear trends in annual mean total O<sub>3</sub> and tagged O<sub>3</sub> tracers that had significant effects on the standard simulation averaged over all of Japan in all simulations are shown and compared in Fig. 9. Simulation A showed no obvious increasing trend in total O<sub>3</sub> over Japan. The surface temperature over Japan in the model that was assimilated into NCEP/NCAR reanalysis data showed a warming of 0.44 ± 0.21 °C decade<sup>-1</sup> in the annual mean during the simulation period, which corresponded well to the observed warming of 0.45 ± 0.23 °C decade<sup>-1</sup> (JMA, 2017). The IAV of the surface temperature was well captured by the model too, although the modeled temperature was somewhat warmer than the observation in the 2000s, particularly

**Table 2.** Summary of the sensitivity simulations and the standard simulation.

Simulation code	CH <sub>4</sub> concentration	O <sub>3</sub> precursor emissions				Stratospheric O <sub>3</sub> trend
		CHN	KOR	JPN	ROW <sup>a</sup>	
A	1980 <sup>b</sup>	1980	1980	1980	1980	1980
B	increase <sup>c</sup>	1980	1980	1980	1980	1980
C	increase	Var <sup>d</sup>	1980	1980	1980	1980
D	increase	Var	Var	1980	1980	1980
E	increase	Var	Var	Var	1980	1980
F (standard)	increase	Var	Var	Var	Var	Var

<sup>a</sup> Precursor emissions in the rest of the world (ROW) other than CHN, KOR, and JPN. <sup>b</sup> Each factor was fixed at the year 1980 level. <sup>c</sup> CH<sub>4</sub> concentration increased until 2000 and flattened thereafter. <sup>d</sup> Temporal variation (Var) of each factor was considered.

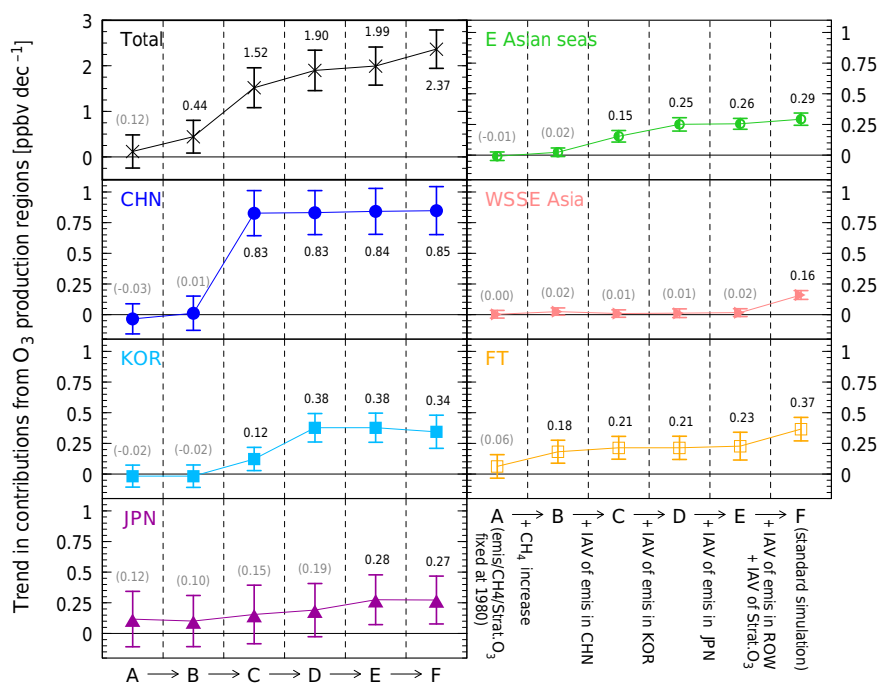


**Figure 9.** Linear trends in the annual mean contributions in 1980–2005 from source regions to surface O<sub>3</sub> over Japan in the sensitivity simulations and the standard simulation (error bars are 95 % confidence intervals). The exact values of the trends are also shown in the figure; the trends without sufficient statistical significance are shown in parentheses. The trends in each region's contribution in the simulations A–E and F (the standard simulation) are arranged from left to right in each panel.

in winter, which might be related to the slight overestimation of winter surface O<sub>3</sub> in the model depicted in Fig. 5. The JPN and total FT contributions exhibited increasing trends (0.12 and 0.06 ppbv decade<sup>-1</sup>, respectively), likely due to the IAV of the climate, but they were non-significant.

The increase in atmospheric concentration of CH<sub>4</sub> was added in simulation B because this would have a non-negligible impact on tropospheric O<sub>3</sub> (background O<sub>3</sub> in particular), as frequently reported (Brasseur et al., 2006; Kawase et al., 2011; HTAP, 2010, and references therein). In the simulations other than A, we used a CH<sub>4</sub> concen-

tration increase rate of about 12.3 ppbv yr<sup>-1</sup> (0.73 % yr<sup>-1</sup>) during 1980–2000 and flattened thereafter. In simulation B, the contribution of the total FT showed a significant increasing trend (0.18 ppbv decade<sup>-1</sup>) as did that of Remote (0.08 ppbv decade<sup>-1</sup>; data not shown). The contributions of several other regions such as CHN, the E Asian seas, and WSSE Asia also showed slight increasing trends (approximately 0.01–0.02 ppbv decade<sup>-1</sup>), although they are non-significant. Note that these values included the impact of CH<sub>4</sub> increase as well as the IAV of the climate increase and, consequently, the total O<sub>3</sub> in simulation B showed a signifi-

cant increasing trend in about  $0.44 \text{ ppbv decade}^{-1}$ , representing about 19 % of the increasing trend in total  $\text{O}_3$  in the standard simulation ( $2.37 \text{ ppbv decade}^{-1}$ ).

In simulations C–E, the temporal variations in emission of  $\text{O}_3$  precursors in northeast Asian regions were gradually added: CHN, KOR, and JPN, respectively. The increase in emissions of  $\text{O}_3$  precursors in CHN in simulation C caused a large significant increasing trend in the contribution of CHN itself ( $0.83 \text{ ppbv decade}^{-1}$ ). Moreover, the emission increase in CHN also had a large impact on the contributions of other regions. In particular, the increasing trends in the contributions of KOR and the E Asian seas became significant:  $0.12$  and  $0.15 \text{ ppbv decade}^{-1}$ , respectively. The JPN and the total FT contributions also showed somewhat larger increasing trends in simulation C than in B, but the growth in trends between the two simulations was not as large as those of KOR and the E Asian seas. The total effect of the emission increase in CHN on the increasing trend in surface  $\text{O}_3$  over Japan, assessed using the difference in total  $\text{O}_3$  trend between simulations B and C, was about  $1.08 \text{ ppbv decade}^{-1}$  and corresponded to about 46 % of the increasing trend in total  $\text{O}_3$  in the standard simulation. The relative contribution of CHN as a source region of  $\text{O}_3$  production to the surface  $\text{O}_3$  increasing trend over Japan was estimated as 36 % in the preceding section (Sect. 3.2); however, the contribution of CHN as a source region of  $\text{O}_3$  precursors emission was somewhat (10 %) larger due to the production of  $\text{O}_3$  outside CHN. It is noteworthy that the slight increasing trend in the contribution of WSSE Asia shown in the  $\text{CH}_4$  increase in simulation B was smaller in simulation C. The contributions of Remote and the stratosphere showed similar responses. The increase in  $\text{O}_3$  precursor emissions in CHN seemed to partly offset the increase in influence of long-range transport of  $\text{O}_3$  from such regions.

The increase in emissions from KOR in addition to CHN in simulation D gave rise to a much larger increasing trend in the contributions of KOR itself ( $0.38 \text{ ppbv decade}^{-1}$ ). Compared with simulation C ( $0.12 \text{ ppbv decade}^{-1}$ ), about one-third of the increasing trend in the contribution of KOR was attributed to the  $\text{O}_3$  precursor emission increase in CHN and the rest to emission increase in KOR. Similarly, the emission increase in KOR caused a larger increasing trend in the contributions of the E Asian seas in simulation D ( $0.25 \text{ ppbv decade}^{-1}$ ). We attributed about half of the increasing trend in the contribution of the E Asian seas in the standard simulation ( $0.29 \text{ ppbv decade}^{-1}$ ) to the impact of  $\text{O}_3$  precursor emission increase in CHN (and partly that of the  $\text{CH}_4$  increase:  $0.15 \text{ ppbv decade}^{-1}$ ) as shown in simulation C, about one-third to that in KOR, and the rest to that in regions other than northeast Asia. By further adding the temporal variation in the domestic (JPN) emissions in simulation E, the increasing trend in the domestic contribution became significant ( $0.28 \text{ ppbv decade}^{-1}$ ), implying that the increasing trend in domestically produced  $\text{O}_3$  was from a combination of multiple factors, each of which did not cause a

significant increase. The total effect of the emission increase in KOR on the increasing trend in surface  $\text{O}_3$  over Japan assessed as the difference between simulations C and D was about  $0.38 \text{ ppbv decade}^{-1}$ . That of the IAV of domestic emissions in Japan, assessed as the difference between simulations D and E, was about  $0.09 \text{ ppbv decade}^{-1}$ . The IAV of domestic emissions in KOR and JPN could account for about 16 and 4 %, respectively, of the increasing trend in total  $\text{O}_3$  in the standard simulation.

The IAV in emissions of  $\text{O}_3$  precursors in northeast Asian regions (CHN, KOR, and JPN) together with the IAV in the climate and the increase in  $\text{CH}_4$  concentration induced a significant increasing trend in total  $\text{O}_3$  over Japan with a rate of  $1.99 \text{ ppbv decade}^{-1}$ . This accounted for about 84 % of the increasing trend in total  $\text{O}_3$  in the standard simulation. The rest of the increasing trend should be regarded as from  $\text{O}_3$  precursor emission changes in regions other than northeast Asia. The difference between simulations E and F (standard simulation) showed that the emission change in such regions influenced surface  $\text{O}_3$  over Japan mainly through increasing the  $\text{O}_3$  production in WSSE Asia and the FT (Fig. 9).

#### 4 Summary and conclusion

We demonstrated the relative importance of the regions of photochemical  $\text{O}_3$  production in the global atmosphere in the long-term increasing trend in surface  $\text{O}_3$  over Japan reported in recent decades by conducting a series of tracer-tagging simulations using the global CTM CHASER. The impact of the IAVs of climate,  $\text{CH}_4$  concentration, and emission of  $\text{O}_3$  precursors ( $\text{NO}_x$  and NMVOC) in different source regions on regional photochemical  $\text{O}_3$  production was also investigated.

The observed increasing trend in surface  $\text{O}_3$  over Japan for 1980–2005 ( $2.70 \text{ ppbv decade}^{-1}$  for annual mean over whole Japan) was successfully reproduced by the model ( $2.58 \text{ ppbv decade}^{-1}$ ), including an obvious tendency of increase toward western Japan and to be greater in the warm season (spring–summer) than in the cold season (fall–winter).

The absolute contribution of each photochemical  $\text{O}_3$  production region to the surface  $\text{O}_3$  over Japan represented by the concentrations of tagged  $\text{O}_3$  tracer showed different temporal evolution by region. The contributions of all Asian regions except the northern part (i.e., CHN, KOR, the E Asian seas, JPN, and WSSE) as well as those of the total FT exhibited significant increasing trends during the period. The increasing trend in the contribution of domestically produced  $\text{O}_3$  in Japan (i.e., JPN) did not differ much among the different regions in Japan. However, there was a tendency in the increasing trends in contributions of CHN, KOR, and the E Asian seas to be large toward western Japan, which was a main cause of the same tendency in the increasing trend in total  $\text{O}_3$  and suggested a large impact of intra-regional transboundary air pollution in East Asia.

The trends in contributions of most O<sub>3</sub> production regions, except JPN, were larger in the warm season than in the cold season, providing a basis for the seasonality in the increasing trend in total O<sub>3</sub> over Japan. Thus, the larger increasing trend in total O<sub>3</sub> in spring than in summer was mainly due to the same tendency in increasing trends in the contributions of northeast Asian regions (CHN, KOR, and JPN), although this was partly compensated for by larger increasing trends in the FT and WSSE Asia contributions in summer than spring. In the cold season, the contributions of FT, WSSE Asia, and Remote had larger increasing trends in winter than in fall, which led to a larger increasing trend in total O<sub>3</sub> in winter than in fall.

The sum of the trends in contributions of O<sub>3</sub> production regions with sufficient statistical significance accounted for most (about 97 %) of the increasing trend in total O<sub>3</sub> over Japan (2.37 ppbv decade<sup>-1</sup>). The largest portion was attributed to the increasing trend in O<sub>3</sub> produced in CHN (36 %; 0.85 ppbv decade<sup>-1</sup>), followed by that in the total FT (16 %; 0.37 ppbv decade<sup>-1</sup>). The increasing trend in contributions of the other northeast Asian regions (KOR, E Asian seas, and JPN; 0.27–0.34 ppbv decade<sup>-1</sup>) each accounted for about 12–15 % of the total O<sub>3</sub> trend, and the majority of the rest of the total O<sub>3</sub> trend (7 %; 0.16 ppbv decade<sup>-1</sup>) was attributable to WSSE Asia.

We further investigated the impact of the temporal variation in controlling factors, such as climate, CH<sub>4</sub> concentration, and emission of O<sub>3</sub> precursors, on photochemical O<sub>3</sub> production in different source regions and its influence on the long-term increasing trend in surface O<sub>3</sub> over Japan through a series of sensitivity simulations that gradually added the temporal variation in these factors. The IAV of the climate and the increase in CH<sub>4</sub> concentration together caused the increase in photochemical O<sub>3</sub> production in several regions and resulted in the significant increasing trend in surface O<sub>3</sub> over Japan (0.44 ppbv decade<sup>-1</sup>) and represented about 19 % of the increasing trend in surface O<sub>3</sub> in the standard simulation. The increase in emission of O<sub>3</sub> precursors in CHN led to the increase in photochemical O<sub>3</sub> production in northeast Asian regions including CHN itself, KOR, JPN, and the E Asian seas. The resulting increasing trend in surface O<sub>3</sub> over Japan (1.08 ppbv decade<sup>-1</sup>) accounted for about 46 % of that in the standard simulation. The relative contribution of CHN to the surface O<sub>3</sub> increasing trend over Japan as the source region of O<sub>3</sub> precursor emission was 10 % larger than as the source region of O<sub>3</sub> production due to production of O<sub>3</sub> outside of CHN. Then, the impact of the O<sub>3</sub> precursor emission change in KOR and JPN on the increasing trend in surface O<sub>3</sub> over Japan (about 0.38 and 0.10 ppbv decade<sup>-1</sup>, respectively) corresponded to 16 and 4 % of the increasing trend in total O<sub>3</sub> in the standard simulation, respectively. The rest of the increasing trend in total O<sub>3</sub> in the standard simulation (about 16 %) was attributed to O<sub>3</sub> precursor emission change in regions other than northeast Asia, mainly through increas-

ing the photochemical O<sub>3</sub> production in WSSE Asia and the total FT.

The results summarized above depended largely on the forcings of long-term simulation, particularly the long-term variation in the emissions of O<sub>3</sub> precursors in Asia. Zhao et al. (2013) estimated the NO<sub>x</sub> emission in China for the period 1995–2010 and compared it to the existing emission inventories, including Hao et al. (2002), Zhang et al. (2007), and the version of REAS used in this study. They showed that the long-term increasing trend in Chinese NO<sub>x</sub> emission in REAS was consistent with that in the other inventories, but the amount of emission was somewhat smaller in REAS than in the others. Therefore, the long-term increasing trend in the contribution of Chinese emission to the surface O<sub>3</sub> over Japan showed in the present study would be retained if the other emission inventories were used for the simulation but the specific values of the contributions could be affected. Further studies should address the impact of these uncertainties in the different emission inventories on the trend in surface O<sub>3</sub> over Japan.

*Data availability.* All the data for the simulation by CHASER used in this publication can be accessed by contacting the author Tatsuya Nagashima (nagashima.tatsuya@nies.go.jp). The AEROS observation is available through the following link: <https://www.nies.go.jp/igreen>.

**The Supplement related to this article is available online at <https://doi.org/10.5194/acp-17-8231-2017-supplement>.**

*Competing interests.* The authors declare that they have no conflict of interest.

*Acknowledgements.* This research was supported by the Global Environment Research Fund (S-7) by the Ministry of the Environment (MOE) of Japan and the East Asian Environmental Research Program at the National Institute for Environmental Studies (NIES). We acknowledge the entire staff of the EANET and the AEROS air quality monitoring stations of the MOE of Japan and of the local governments for carrying out measurements and providing the observations. The calculations were performed on the NIES supercomputer system (NEC SX-8R, and SX9). The GFD-DENNOU library was used for drawing the figures.

Edited by: Qiang Zhang

Reviewed by: two anonymous referees

## References

- Akimoto, H., Mori, Y., Sasaki, K., Nakanishi, H., Ohizumi, T., and Itano, Y.: Analysis of monitoring data of ground-level ozone in Japan for longterm trend during 1990–2010: Causes of temporal and spatial variation, *Atmos. Environ.*, 102, 302–310, 2015.
- Akiyoshi, H., Zhou, L. B., Yamashita, Y., Sakamoto, K., Yoshiki, M., Nagashima, T., Takahashi, T., Kurokawa, J., Takigawa, M., and Imamura, T.: A CCM simulation of the breakup of the Antarctic polar vortex in the years 1980–2004 under the CCMVal scenarios, *J. Geophys. Res.*, 114, D03103, <https://doi.org/10.1029/2007JD009261>, 2009.
- Brasseur, G. P., Schultz, M., Granier, C., Saunois, M., Diehl, T., Botzet, M., and Roeckner, E.: Impact of climate change on the future chemical composition of the global troposphere, *J. Climate*, 19, 3932–3951, <https://doi.org/10.1175/JCLI3832.1>, 2006.
- Chang, S.-C. and Lee, C.-T.: Evaluation of the trend of air quality in Taipei, Taiwan from 1994 to 2003, *Environ. Monit. Assess.*, 127, 87–96, <https://doi.org/10.1007/s10661-006-9262-1>, 2007.
- Chou, C. C.-K., Liu, S. C., Lin, C.-Y., Shiu, C.-J., and Chang, K.-H.: The trend of surface ozone in Taipei, Taiwan, and its causes: Implications for ozone control strategies, *Atmos. Environ.*, 40, 3898–3908, 2006.
- Cooper, O. R., Parrish, D. D., Ziemke, J., Balashov, N. V., Cupeiro, M., Galbally, I. E., Gilge, S., Horowitz, L., Jensen, N. R., Lamarque, J.-F., Naik, V., Oltmans, S. J., Schwab, J., Shindell, D. T., Thompson, A. M., Thouret, V., Wang, Y., and Zbinden, R. M.: Global distribution and trends of tropospheric ozone: An observation-based review, *Elementa*, 2, 000029, <https://doi.org/10.12952/journal.elementa.000029>, 2014.
- Ding, A. J., Wang, T., Thouret, V., Cammas, J.-P., and Nédélec, P.: Tropospheric ozone climatology over Beijing: analysis of aircraft data from the MOZAIC program, *Atmos. Chem. Phys.*, 8, 1–13, <https://doi.org/10.5194/acp-8-1-2008>, 2008.
- Eyring, V., Harris, N. R. P., Rex, M., Shepherd, T. G., Fahey, D. W., Amanatidis, G. T., Austin, J., Chipperfield, M. P., Dameris, M., Forster, P. M. De F., Gettelman, A., Graf, H. F., Nagashima, T., Newman, P. A., Pawson, S., Prather, M. J., Pyle, J. A., Salawitch, R. J., Santer, B. D., and Waugh, D. W.: A strategy for process-oriented validation of coupled chemistry-climate models, *B. Am. Meteorol. Soc.*, 86, 1117–1133, 2005.
- Hao, J. M., Tian, H. Z., and Lu, Y. Q.: Emission inventories of NO<sub>x</sub> from commercial energy consumption in China, 1995–1998, *Environ. Sci. Technol.*, 36, 552–560, <https://doi.org/10.1021/Es015601k>, 2002.
- HTAP, UNECE: Hemispheric Transport of Air Pollution 2010: Part A: Ozone and Particulate Matter, Air Pollution Studies No. 17, edited by: Dentener, F., Keating, T., and Akimoto, H., United Nations Publication, Geneva, Switzerland ECE/EN.Air/100, 2010.
- JMA (Japan Meteorological Agency): available at: [http://www.data.jma.go.jp/cpdinfo/temp/list/an\\_jpn.html](http://www.data.jma.go.jp/cpdinfo/temp/list/an_jpn.html), last access: 3 July 2017 (in Japanese).
- Kalnay, E., Kanamitsu, M., Kistler, R., Collins, W., Deaven, D., Gandin, L., Iredell, M., Saha, S., White, G., Woollen, J., Zhu, Y., Leetmaa, A., Reynolds, B., Chelliah, M., Ebisuzaki, W., Higgins, W., Janowiak, J., Mo, K. C., Ropelewski, C., Wang, J., Jenne, R., and Joseph, D.: The NCEP/NCAR 40-year reanalysis project, *B. Am. Meteorol. Soc.*, 77, 437–470, 1996.
- Kawase, H., Nagashima, T., Sudo, K., and Nozawa, T.: Future changes in tropospheric ozone under Representative Concentration Pathways (RCPs), *Geophys. Res. Lett.*, 38, L05801, <https://doi.org/10.1029/2010GL046402>, 2011.
- Kurokawa, J., Ohara, T., Uno, I., Hayasaki, M., and Tanimoto, H.: Influence of meteorological variability on inter-annual variations of springtime boundary layer ozone over Japan during 1981–2005, *Atmos. Chem. Phys.*, 9, 6287–6304, <https://doi.org/10.5194/acp-9-6287-2009>, 2009.
- Kurokawa, J., Ohara, T., Morikawa, T., Hanayama, S., Janssens-Maenhout, G., Fukui, T., Kawashima, K., and Akimoto, H.: Emissions of air pollutants and greenhouse gases over Asian regions during 2000–2008: Regional Emission inventory in ASIA (REAS) version 2, *Atmos. Chem. Phys.*, 13, 11019–11058, <https://doi.org/10.5194/acp-13-11019-2013>, 2013.
- Lee, H.-J., Kim, S.-W., Brioude, J., Cooper, O. R., Frost, G. J., Kim, C.-H., Park, R. J., Trainer, M., and Woo J.-H.: Transport of NO<sub>x</sub> in East Asia identified by satellite and in situ measurements and Lagrangian particle dispersion model simulations, *J. Geophys. Res.-Atmos.*, 119, 2574–2596, <https://doi.org/10.1002/2013JD021185>, 2014.
- Li, H. C., Chen, K. S., Huang, C. H., and Wang, H. K.: Meteorologically adjusted long-term trend of ground-level ozone concentrations in Kaohsiung County, southern Taiwan, *Atmos. Environ.*, 44, 3605–3608, 2010.
- Li, J., Wang, Z., Akimoto, H., Yamaji, K., Takigawa, M., Pochanart, P., Liu, Y., Tanimoto, H., and Kanaya, Y.: Near-ground ozone source attributions and outflow in central eastern China during MTX2006, *Atmos. Chem. Phys.*, 8, 7335–7351, <https://doi.org/10.5194/acp-8-7335-2008>, 2008.
- Lin, Y.-K., Lin, T.-H., and Chang, S.-C.: The changes in different ozone metrics and their implications following precursor reductions over northern Taiwan from 1994 to 2007, *Environ. Monit. Assess.*, 169, 143–157, 2010.
- Logan, J. A., Megretskaia, I. A., Miller, A. J., Tiao, G. C., Choi, D., Zhang, L., Stolarski, R. S., Labow, G. J., Hollandsworth, S. M., Bodeker, G. E., Claude, H., de Muer, D., Kerr, J. B., Tarasick, D. W., Oltmans, S. J., Johnson, B., Schmidlin, F., Staehelin, J., Viatte, P., and Uchino, O.: Trends in the vertical distribution of ozone: A comparison of two analyses of ozonesonde data, *J. Geophys. Res.*, 104, 26373–26399, 1999.
- Lu, W.-Z. and Wang, X.-K.: Evolving trend and self-similarity of ozone pollution in central Hong Kong ambient during 1984–2002, *Sci. Total Environ.*, 357, 160–168, 2006.
- Mauzerall, D. L., Sultan, B., Kim, N., and Bradford, D. F.: NO<sub>x</sub> emissions from large point sources: variability in ozone production, resulting health damages and economic costs, *Atmos. Environ.*, 39, 2851–2866, 2005.
- Meinshausen, M., Smith, S. J., Calvin, K., Daniel, J. S., Kainuma, M. L. T., Lamarque, J.-F., Matsumoto, K., Montzka, S. A., Raper, S. C. B., Riahi, K., Thomson, A., Velders, G. J. M., and van Vuuren, D. P. P.: The RCP greenhouse gas concentrations and their extensions from 1765 to 2300, *Climatic Change*, 109, 213–241, 2011.
- MOE (Ministry of Environment) Japan: FY 2013 status of air pollution, available at: [http://www.env.go.jp/air/osen/jokyo\\_h25](http://www.env.go.jp/air/osen/jokyo_h25) (last access: 3 July 2017), 2013 (in Japanese).
- Nagashima, T., Ohara, T., Sudo, K., and Akimoto, H.: The relative importance of various source regions on East Asian surface ozone, *Atmos. Chem. Phys.*, 10, 11305–11322, <https://doi.org/10.5194/acp-10-11305-2010>, 2010.

- Naja, M. and Akimoto, H.: Contribution of regional pollution and long-range transport to the Asia-Pacific region: Analysis of long-term ozonesonde data over Japan, *J. Geophys. Res.*, 109, D21306, <https://doi.org/10.1029/2004JD004687>, 2004.
- Nozawa, T., Nagashima, T., Shiogama, H., and Crooks, S. A.: Detecting natural influence on surface air temperature change in the early twentieth century, *Geophys. Res. Lett.*, 32, L20719, <https://doi.org/10.1029/2005GL023540>, 2005.
- Ohara, T. and Sakata, T.: Long-term variation of photochemical oxidants over Japan, *Jpn. Soc. Atmos. Environ.*, 38, 47–54, 2003 (in Japanese with English summary).
- Ohara, T., Akimoto, H., Kurokawa, J., Horii, N., Yamaji, K., Yan, X., and Hayasaka, T.: An Asian emission inventory of anthropogenic emission sources for the period 1980–2020, *Atmos. Chem. Phys.*, 7, 4419–4444, <https://doi.org/10.5194/acp-7-4419-2007>, 2007.
- Ohara, T., Yamaji, K., Uno, I., Tanimoto, H., Sugata, S., Nagashima, T., Kurokawa, J., Horii, N., and Akimoto, H.: Long-term simulations of surface ozone in East Asia during 1980–2020 with CMAQ and REAS inventory, in: *Air Pollution Modelling and Its Application XIX (NATO Science for Peace and Security Series C: Environmental Security)*, edited by: Borrego, C. and Miranda, A. I., Springer, Dordrecht, the Netherlands, 136–144, 2008.
- Olivier, J. G. J. and Berdowski, J. J. M.: Global emissions sources and sinks, in: *The Climate System*, edited by: Berdowski, J., Guicherit, R., and Heij, B. J., A. A. Balkema Publishers/Swets & Zeitlinger Publishers, Lisse, the Netherlands, 33–78, 2001.
- Oltmans, S. J., Lefohn, A. S., Harris, J. M., Galbally, I., Scheel, H. E., Bodeker, G., Brunke, E., Claude, H., Tarasick, D., Johnson, B. J., Simmonds, P., Shadwick, D., Anlauf, K., Hayden, K., Schmidlin, F., Fujimoto, T., Akagi, K., Meyer, C., Nichol, S., Davies, J., Redondas, A., and Cuevas, E.: Long-term changes in tropospheric ozone, *Atmos. Environ.*, 40, 3156–3173, 2006.
- Oltmans, S. J., Lefohn, A. S., Shadwick, D., Harris, J. M., Scheel, H. E., Galbally, I., Tarasick, D. W., Johnson, B. J., Brunke, E.-G., Claude, H., Zeng, G., Nichol, S., Schmidlin, F., Davies, J., Cuevas, E., Redondas, A., Naoe, H., Nakano, T., and Kawasato, T.: Recent tropospheric ozone changes – A pattern dominated by slow or no growth, *Atmos. Environ.*, 67, 331–351, 2013.
- Parrish, D. D., Law, K. S., Staehelin, J., Derwent, R., Cooper, O. R., Tanimoto, H., Volz-Thomas, A., Gilge, S., Scheel, H.-E., Steinbacher, M., and Chan, E.: Long-term changes in lower tropospheric baseline ozone concentrations at northern mid-latitudes, *Atmos. Chem. Phys.*, 12, 11485–11504, <https://doi.org/10.5194/acp-12-11485-2012>, 2012.
- Rayner, N. A., Parker, D. E., Horton, E. B., Folland, C. K., Alexander, L. V., Rowell, D. P., Kent, E. C., and Kaplan, A.: Global analyses of sea surface temperature, sea ice, and night marine air temperature since the late nineteenth century, *J. Geophys. Res.*, 108, 4407, <https://doi.org/10.1029/2002JD002670>, 2003.
- Schultz, M. G., Heil, A., Hoelzemann, J. J., Spessa, A., Thonicke, K., Goldammer, J. G., Held, A. C., Pereira, J. M. C., and van het Bolscher, M.: Global wildland fire emissions from 1960 to 2000, *Global Biogeochem. Cy.*, 22, GB2002, <https://doi.org/10.1029/2007GB003031>, 2008.
- Seo, J., Youn, D., Kim, J. Y., and Lee, H.: Extensive spatiotemporal analyses of surface ozone and related meteorological variables in South Korea for the period 1999–2010, *Atmos. Chem. Phys.*, 14, 6395–6415, <https://doi.org/10.5194/acp-14-6395-2014>, 2014.
- Shindell, D., Kuylenstierna, J. C. I., Faluvegi, G., Milly, G., Emberson, L., Hicks, K., Vignati, E., Van Dingenen, R., Janssens-Maenhout, G., Raes, F., Pozzoli, L., Amann, M., Klimont, Z., Kupiainen, K., Höglund-Isaksson, L., Anenberg, S. C., Müller, N., Schwartz, J., Streets, D., Ramanathan, V., Oanh, N. T. K., Williams, M., Demkine, V., and Fowler, D.: Simultaneously mitigating near-term climate change and improving human health and food security, *Science*, 335, 183–189, 2012.
- Silva, R. A., West, J. J., Zhang, Y., Anenberg, S. C., Lamarque, J.-F., Shindell, D. T., Collins, W. J., Dalsoren, S., Faluvegi, G., Folberth, G., Horowitz, L. W., Nagashima, T., Naik, V., Rumbold, S., Skeie, F., Sudo, K., Takemura, T., Bergmann, D., Cameron-Smith, P., Cionni, I., Doherty, R. M., Eyring, V., Josse, B., MacKenzie, I. A., Plummer, D., Righi, M., Stevenson, D. S., Strode S., Szopa, S., and Zeng, G.: Global premature mortality due to anthropogenic outdoor air pollution and the contribution of past climate change, *Environ. Res. Lett.*, 8, 034005, <https://doi.org/10.1088/1748-9326/8/3/034005>, 2013.
- Sudo, K. and Akimoto, H.: Global source attribution of tropospheric ozone: Long-range transport from various source regions, *J. Geophys. Res.*, 112, D12302, <https://doi.org/10.1029/2006JD007992>, 2007.
- Sudo, K., Takahashi, M., Kurokawa, J., and Akimoto, H.: CHASER: A global chemical model of the troposphere: 1. Model description, *J. Geophys. Res.*, 107, 4339, <https://doi.org/10.1029/2001JD001113>, 2002.
- Susaya, J., Kim, K.-H., Shon, Z.-H., and Brown, R. J. C.: Demonstration of long-term increases in tropospheric O<sub>3</sub> levels: Causes and potential impacts, *Chemosphere*, 92, 1520–1528, 2013.
- Tanimoto, H.: Increase in springtime tropospheric ozone at a mountainous site in Japan for the period 1998–2006, *Atmos. Environ.*, 43, 1358–1363, 2009.
- Tanimoto, H., Ohara, T., and Uno, I.: Asian anthropogenic emissions and decadal trends in springtime tropospheric ozone over Japan: 1998–2007, *Geophys. Res. Lett.*, 36, L23802, <https://doi.org/10.1029/2009GL041382>, 2009.
- UNEP (United Nations Environment Programme) and WMO (World Meteorological Organization): Integrated Assessment of Black Carbon and Tropospheric Ozone: Summary for Decision Makers, available at: <https://wedocs.unep.org/rest/bitstreams/12809/retrieve> (last access: 3 July 2017), 2011.
- US EPA (U.S. Environmental Protection Agency): Air Quality Criteria for Ozone and Related Photochemical Oxidants (Final), U.S. Environmental Protection Agency, Washington, DC, EPA/600/R-05/004aF-cF, 2006.
- Van Aardenne, J. A., Dentener, F. J., Olivier, J. G. J., Klein Goldewijk, C. G. M., and Lelieveld, J.: A 1 × 1 degree resolution dataset of historical anthropogenic trace gas emissions for the period 1890–1990, *Global Biogeochem. Cy.*, 15, 909–928, 2001.
- Wakamatsu, S., Morikawa, T., and Ito, A.: Air Pollution Trends in Japan between 1970 and 2012 and Impact of Urban Air Pollution Countermeasures, *Asian J. Atmos. Environ.*, 7, 177–190, 2013.
- Wang, T., Wei, X. L., Ding, A. J., Poon, C. N., Lam, K. S., Li, Y. S., Chan, L. Y., and Anson, M.: Increasing surface ozone concentrations in the background atmosphere of Southern China, 1994–2007, *Atmos. Chem. Phys.*, 9, 6217–6227, <https://doi.org/10.5194/acp-9-6217-2009>, 2009.
- Wang, X. and Mauzerall, D. L.: Characterizing distributions of surface ozone and its impact on grain production in China, Japan

- and South Korea: 1990 and 2020, *Atmos. Environ.*, 38, 4383–4402, 2004.
- Wang, Y., Zhang, Y., Hao, J., and Luo, M.: Seasonal and spatial variability of surface ozone over China: contributions from background and domestic pollution, *Atmos. Chem. Phys.*, 11, 3511–3525, <https://doi.org/10.5194/acp-11-3511-2011>, 2011.
- Xu, X., Lin, W., Wang, T., Yan, P., Tang, J., Meng, Z., and Wang, Y.: Long-term trend of surface ozone at a regional background station in eastern China 1991–2006: enhanced variability, *Atmos. Chem. Phys.*, 8, 2595–2607, <https://doi.org/10.5194/acp-8-2595-2008>, 2008.
- Zhang, Q., Streets, D. G., He, K., Wang, Y., Richter, A., Burrows, J. P., Uno, I., Jang, C. J., Chen, D., Yao, Z., and Lei, Y.: NO<sub>x</sub> emission trends for China, 1995–2004: The view from the ground and the view from space, *J. Geophys. Res.-Atmos.*, 112, D22306, <https://doi.org/10.1029/2007jd008684>, 2007.
- Zhang, Q., Yuan, B., Shao, M., Wang, X., Lu, S., Lu, K., Wang, M., Chen, L., Chang, C.-C., and Liu, S. C.: Variations of ground-level O<sub>3</sub> and its precursors in Beijing in summertime between 2005 and 2011, *Atmos. Chem. Phys.*, 14, 6089–6101, <https://doi.org/10.5194/acp-14-6089-2014>, 2014.
- Zhao, B., Wang, S. X., Liu, H., Xu, J. Y., Fu, K., Klimont, Z., Hao, J. M., He, K. B., Cofala, J., and Amann, M.: NO<sub>x</sub> emissions in China: historical trends and future perspectives, *Atmos. Chem. Phys.*, 13, 9869–9897, <https://doi.org/10.5194/acp-13-9869-2013>, 2013.